THE ASTRONOMICAL JOURNAL, ACCEPTED FOR THE 2003 DECEMBER ISSUE
Preprint typeset using LATEX style emulateapj v. 7/8/03

arXiv:astro-ph/0308278v1 15 Aug 2003

THE X-RAY PROPERTIES OF THE NEARBY STAR-FORMING GALAXY IC 342: THE *XMM-NEWTON* VIEW

F. E. BAUER,[1] W. N. BRANDT,[1] AND B. LEHMER[1]

The Astronomical Journal, accepted for the 2003 December issue

ABSTRACT

We present results on the X-ray properties of IC 342 using a 10 ks *XMM-Newton* observation. Thirty-five sources are detected coincident with the disk of IC 342 (more than tripling the number known), of which ≈ 31 are likely to be intrinsic to IC 342. This point-source population exhibits a diverse range of spectral properties and has an X-ray luminosity function slope and infrared luminosity comparable to that of starburst galaxies such as M82 and the Antennae, while its relative lack of extended X-ray emission is similar to the properties of quiescent spirals. Although we find no evidence for short-term variability in any of the X-ray sources, we do detect long-term variability between this observation and the 1991 *ROSAT* and 1993/2000 *ASCA* observations for five sources. Notably, the second most luminous source in IC 342 (X-2) is found to have an absorption-corrected 0.5–10 keV luminosity of 5.75×10^{39} erg s^{-1} and a spectrum best-fit by an absorbed multi-color accretion-disk model with $T_{\rm in} = 2.17^{+0.25}_{-0.12}$ keV and $N_{\rm H} = (15.3^{+1.9}_{-1.8}) \times 10^{21}$ cm^{-2}. This is the lowest luminosity state observed for X-2 to date, although the slope of the spectrum is intermediate between the previously observed low/hard and high/soft states. IC 342 X-1, on the other hand, is found to be in an identical state to that observed in 2000 with *ASCA*. Assuming X-1 is in an anomalous very high (VH) state, then either (1) X-1 has remained in this state between 2000 and 2002, and is therefore the longest duration VH-state binary ever observed, or (2) it was simply caught in a VH state by chance in both the 2000 *ASCA* and 2002 *XMM-Newton* observations. We have also confirmed the *ROSAT* HRI result that the nucleus of IC 342 is made up of both point-like and extended emission, with the extended emission contributing ≈55% and ≈35% in the 0.3–2.0 keV and 2.0–10.0 keV bands, respectively. The spectrum of the nucleus is best fit by an absorbed two-component model consisting of a thermal plasma with a temperature of $kT \approx 0.3$ and a power law with a photon index of $\Gamma \approx 2.53$. The relative fluxes of the two spectral components suggest that the nucleus is complex, with a soft extended component contributing approximately half of the total luminosity.

Subject headings: galaxies: active — galaxies: general — X-rays: binaries — X-rays: galaxies

1. INTRODUCTION

IC 342 is a nearby, nearly face-on ($i \sim 20^\circ$) Scd galaxy with spiral arms undergoing moderate star formation and an intense starburst core. It has an absolute visual magnitude of $M_V \approx -21.3$, an optical D_{25} diameter of $\approx 29.7'$, and neutral hydrogen and total dynamical masses of $M_{\rm HI} = 2.1 \times 10^9\ M_\odot$ and $M_{\rm tot} = 1.1 \times 10^{11}\ M_\odot$, respectively (Tully & Fisher 1988; Crosthwaite et al. 2000). Although the Galactic absorption column density toward IC 342 is relatively large ($N_{\rm H} = 3 \times 10^{21}$ cm^{-2}; Stark et al. 1992), it has been observed by *Einstein*, *ROSAT*, and *ASCA*. *ROSAT* High Resolution Imager (HRI) observations ($\theta_{\rm FWHM} \approx 5''$) resolved the disk of the galaxy into a collection of ten point sources above a 0.1–2.5 keV flux limit of $\approx 3 \times 10^{-14}$ erg cm^{-2} s^{-1} (or an absorption-corrected luminosity limit of $\approx 2 \times 10^{37}$ erg s^{-1}; Bregman et al. 1993, hereafter BCT93).[2] *ROSAT* and *ASCA* measurements indicate that the bulk of the X-ray emission arises from four ultraluminous X-ray sources (ULXs, $L_{\rm X} \approx 10^{39}$–$10^{40}$ erg s^{-1}), one of which is coincident with the nucleus (BCT93; Okada et al. 1998, hereafter O98; Kubota et al. 2001, hereafter K01). Two *ASCA* observations (38 ks in 1993, 276 ks in 2000) have shown the ULXs to vary both in intensity and spectral shape (O98; K01; Sugiho et al. 2001), suggesting that they are single objects with masses of ≈ 10–$100\ M_\odot$ (if radiating isotropically below their Eddington limits). The nucleus, however, has remained constant and appears to be slightly extended (BCT93). Since this extended emission encompasses the surface-brightness enhancements seen at optical-to-radio wavelengths (≈ 10–$15''$) that are attributed to a high rate of ongoing star formation, BCT93 speculated that the emission might be from a hot gas bubble.

Here we report results from a 10 ks *XMM-Newton* observation of IC 342. This observation provides the highest resolution and most sensitive hard X-ray imaging of IC 342 published to date, as well as a field of view which covers the entire extent of the galaxy. We describe the observation and reduction of the X-ray data in §2, provide the basic X-ray properties of the detected sources in the context of previous results in §3, and summarize our findings in §4.

2. XMM–NEWTON OBSERVATION AND DATA ANALYSIS

IC 342 was observed on 2001 February 11 for ≈10 ks with the PN–CCD camera (Strüder et al. 2001) and the two MOS–CCD cameras (Turner et al. 2001) using the medium filter. The nucleus of IC 342 was placed at the aimpoint, allowing the entire optical extent of the galaxy to be imaged. The processing, screening, and analysis of the data were performed using the standard tools from `SAS` (v.5.3.3) and `CIAO` (v2.3), as well as custom `IDL` software. The raw MOS and PN data were initially processed using the standard *epchain* and *emchain* pipeline scripts. Time intervals contaminated by soft-proton flares were identified using the background light curve in the 10–13 keV band. Approximately 200 s of exposure was excluded at the end of the observation due to flaring; the background for the rest of the observation remained relatively constant at $\lesssim 0.2$ counts s^{-1}. Our final exposures were 9488 s,

---

[1] Department of Astronomy & Astrophysics, 525 Davey Lab, The Pennsylvania State University, University Park, PA 16802.

[2] We adopt a distance of 3.3 ± 0.3 Mpc to IC 342, based on the period-luminosity relation of 20 Cepheid variables (Saha et al. 2002). Results from other papers have been corrected to this distance.

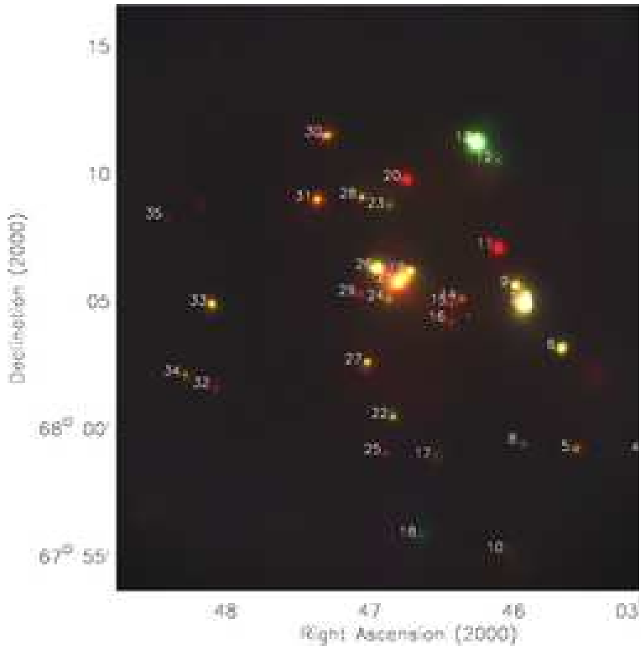

FIG. 1.— An *XMM-Newton* "false-color" $25' \times 25'$ image of IC 342 with red, green, and blue representing 0.3–2.0 keV, 2.0–5.0 keV, and 5.0–10 keV emission, respectively. Prior to combination, each image was smoothed with an adaptive-kernel algorithm (Ebeling et al. 2003). Little diffuse emission is observed. In addition to a bright nuclear component (source 21), 34 off-nuclear point sources are detected. The sources have been labeled according to their source number in Table 1.

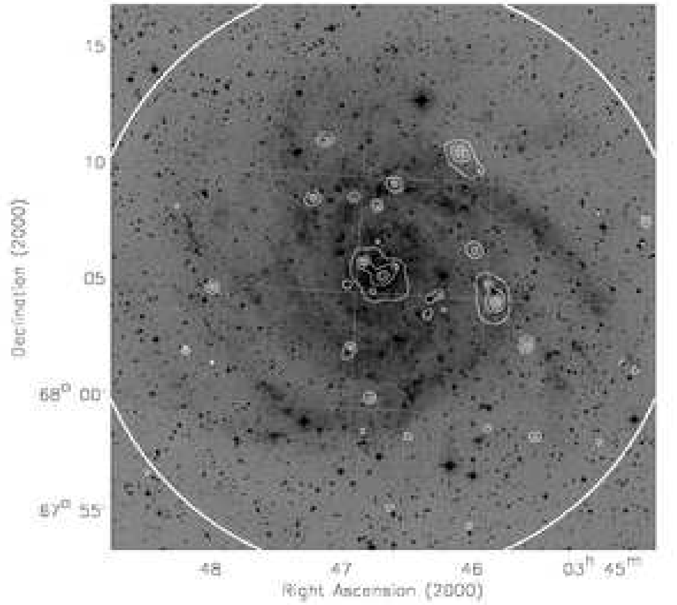

FIG. 2.— A $25' \times 25'$ Digitized Sky Survey B_J-band image with *XMM-Newton* contours superimposed. Contours are calculated from the combined MOS image for the 0.3–10 keV band. The lowest contour indicates 0.33 counts pixel^{-1} ($\approx 3\times$ the average background value), with each subsequent contour increasing by a factor of four. All sources lie within the white $12'$ radius circle shown.

9507 s, and 4888 s for the MOS1, MOS2, and PN detectors, respectively. We selected only good event patterns: $\leq$12 for MOS imaging and spectroscopy, $\leq$12 for PN imaging, and $\leq$4 for PN spectroscopy.

Source detection was initially performed on the MOS and PN images in the 0.3–10 keV band using the standard `SAS` *eboxdetect* and *emldetect* algorithms. A likelihood value of 10 was imposed, corresponding to a significance level of $\approx 3.6\sigma$. Thirty sources were detected, although we found that several apparent sources — including two with $\gtrsim$100 MOS+PN counts — were detected by *eboxdetect* but rejected by *emldetect*.[3] As a cross-check, we compared the sources found using *eboxdetect* with those found using the `CIAO` *wavdetect* algorithm (Freeman et al. 2002), run on the merged MOS+PN image with a significance threshold of 1×10^{-7}. We found good agreement between the algorithms, and we have chosen the 35 sources common to both methods as our X-ray point-source sample. Table 1 lists the basic X-ray properties of these sources, while Figure 1 indicates their position in the X-ray image. Background-subtracted counts were extracted using circular apertures ranging in radius from $\approx$17–68$''$, depending on off-axis angle and the relative brightness of the source compared to the local background. Local backgrounds were determined after removal of the 35 point sources. Our background-subtracted detection limit is $\approx$ 25 MOS+PN counts, corresponding to an absorbed 0.3–10 keV flux of $\approx (1\text{–}2) \times 10^{-14}$ erg cm^{-2} s^{-1}.

We have more than tripled the number of known X-ray sources spatially coincident with IC 342, compared to the *ROSAT* HRI observation reported by BCT93 of similar soft-band depth, thanks to the high-energy response of *XMM-Newton*. Figure 2 shows X-ray contours overlaid on an optical image of IC 342, indicating that the majority of the X-ray sources coincide with the spiral arms of the galaxy.

The nominal astrometric accuracy for *XMM-Newton* is $\approx 4''$ (e.g., Jansen et al. 2001). We have improved upon this somewhat by matching X-ray sources to optical sources from the *r*-band image of Saha et al. (2002) and the United States Naval Observatory B1.0 catalog (USNOB1; Monet et al. 2003).[4] X-ray matching to optical sources was performed using a $4''$ matching radius, with 13 sources having potential optical counterparts: the nucleus of IC 342, four spatially extended sources (potential H II regions), five faint point sources with $R \sim 21$–25 within the spiral arms of IC 342, and three bright foreground stars with $R \sim 11$–13. Excluding the five faint point sources that potentially could be chance alignments, we find average *XMM-Newton* Right Ascension and Declination offsets of $\approx -3.''4$ and $0.''4$, respectively, resulting in a registration accuracy of $\approx 1.''3$ rms; positions have been corrected for these offsets throughout. These offsets do not change significantly (only by $0.''3$) if we align the X-ray and optical images using only the three bright stars and the nucleus (i.e., the most secure matches). Although we have limited statistics, we find no obvious rotation of the X-ray image to within our registration errors.

Because IC 342 has a large angular extent and lies at low Galactic latitude ($b = 10.^\circ58$), the chance superposition of Galactic X-ray sources and background AGN is a concern. Fortunately, IC 342 has a Galactic longitude of $l = 138.^\circ17$, so our line-of-sight is relatively far from the Galactic Center and therefore intersects only a relatively small fraction of the Galaxy. Based on the numbers of serendipitous sources detected in four archival observations within 15° of IC 342

---

[3] These sources are noted in Table 1.

[4] The *r*-band image was astrometrically registered to an accuracy of $\approx 0.''1$ RMS using 216 stars from the Tycho-2 and Guide Star v2.2 catalogs.

TABLE 1. X-RAY SOURCES SPATIALLY COINCIDENT WITH IC 342

(1) ID	(2) Source Name XMMU J	(3) Other Names	(4) Off-Axis ′	(5) Counts	(6) BR	(7) F_X	(8) L_X	(9) R	(10) $\log(F_X/F_O)$	(11) HRI F_X	(12) Optical ID
1	034448.3+680843		11.6	$107.3^{+13.7}_{-11.8}$	$0.54^{+0.16}_{-0.14}$	14.20	2.43	$\gtrsim 20$	$\gtrsim 0.65$	<3.74	
2*	034449.4+680738		11.3	$22.8^{+9.3}_{-7.4}$	< 0.98	0.21	Galactic	13.0	–3.98	<3.17	Star ($1.''5$)
3	034449.7+680214		11.7	$39.8^{+11.2}_{-9.3}$	$1.29^{+0.75}_{-0.61}$	3.78	0.65	$\gtrsim 20$	$\gtrsim 0.08$	<2.46	
4	034505.1+675904		11.8	$28.1^{+9.3}_{-7.4}$	$1.43^{+0.99}_{-0.78}$	0.92	0.16	$\gtrsim 20$	$\gtrsim -0.54$	<2.74	
5	034534.7+675908†	R1	9.6	$87.1^{+12.9}_{-11.0}$	$0.74^{+0.23}_{-0.20}$	9.71	1.66	$\gtrsim 20$	$\gtrsim 0.49$	<4.06	
6	034540.2+680308†		6.9	$325.9^{+22.3}_{-20.4}$	$1.22^{+0.17}_{-0.16}$	23.91	5.92	$\gtrsim 20$	$\gtrsim 0.88$	3.16	
7	034556.0+680455	X-1, R3, A1	5.0	$4132.8^{+68.3}_{-66.5}$	$1.07^{+0.04}_{-0.03}$	214.54	50.25	20.1^S	1.96	27.17	Supernova Remnant ($0.''3$; Roberts et al. 2003)
8	034556.8+675926		8.0	$54.1^{+11.2}_{-9.3}$	$0.89^{+0.38}_{-0.32}$	2.96	0.51	$\gtrsim 20$	$\gtrsim -0.03$	<2.48	
9	034559.7+680536		4.6	$324.4^{+20.9}_{-19.1}$	$0.98^{+0.13}_{-0.12}$	20.04	4.69	$\gtrsim 20$	$\gtrsim 0.80$	<4.91	
10	034603.2+675510		11.4	$30.0^{+9.1}_{-7.1}$	$0.56^{+0.43}_{-0.32}$	3.11	0.53	$\gtrsim 20$	$\gtrsim -0.01$	<2.73	
11*	034606.8+680705	R4	4.1	$275.9^{+21.0}_{-19.2}$	$0.04^{+0.04}_{-0.03}$	3.65	Galactic	12.0	–3.05	4.07	Star ($0.''6$)
12	034607.0+681029		6.1	$72.9^{+11.9}_{-10.0}$	$1.70^{+0.57}_{-0.52}$	6.22	1.06	24.7^S	1.17	<2.15	($0.''5$)
13	034616.0+681115	X-2, R5, A2	6.3	$2215.9^{+51.0}_{-49.3}$	$3.41^{+0.19}_{-0.19}$	208.66	50.02	$\gtrsim 24^S$	$\gtrsim 3.48$	12.56	
14	034622.4+680505†		2.6	$55.1^{+11.4}_{-9.5}$	$0.38^{+0.20}_{-0.16}$	6.55	1.12	20.2^S	0.40	<4.17	HII Region? ($1.''3$, also R = 21.8, $1.''9$)
15*	034626.4+680453†		2.3	$37.0^{+10.8}_{-8.9}$	< 0.52	0.34	Galactic	12.9^S	–3.81	<2.44	Star ($2.''3$)
16	034627.2+680414†		2.5	$44.3^{+10.8}_{-8.9}$	$0.26^{+0.20}_{-0.15}$	2.39	0.41	$\sim 21^S$	~ 0.28	<3.13	($0.''2$; complex X-ray source blend with nearby star?)
17	034633.2+675852		7.0	$46.5^{+10.6}_{-8.7}$	$1.10^{+0.51}_{-0.43}$	4.15	0.71	$\gtrsim 20$	$\gtrsim 0.12$	<3.71	
18	034639.6+675548		10.0	$33.7^{+9.4}_{-7.4}$	> 2.92	8.40	1.43	$\gtrsim 20$	$\gtrsim 0.42$	<3.32	Hard X-ray source, possible bkgd. AGN?
19	034643.9+680609	R6	0.6	$402.4^{+22.8}_{-21.0}$	$0.72^{+0.08}_{-0.08}$	14.87	3.51	21.8^S	1.53	2.68	($1.''0$)
20*	034646.0+680946	R7	4.0	$181.2^{+18.3}_{-16.4}$	< 0.15	4.07	Galactic?	21.7^S	0.84	12.85	Star? ($0.''3$)
21	034648.8+680546	X-3, R8, A3	0.0	$2233.1^{+50.2}_{-48.4}$	$0.30^{+0.02}_{-0.02}$	54.16	15.05	$\sim 10^S$	~ -2.7	21.74	Nucleus ($0.''3$)
22	034651.2+680027†		5.3	$108.3^{+14.7}_{-12.9}$	$1.86^{+0.56}_{-0.50}$	7.46	1.27	$\gtrsim 20$	$\gtrsim 0.37$	<2.70	
23	034652.8+680841		2.9	$56.7^{+13.8}_{-11.9}$	$1.49^{+0.84}_{-0.65}$	3.44	0.59	21.9^S	0.80	<2.36	HII Region? ($0.''2$)
24	034652.9+680504		0.8	$106.8^{+13.7}_{-11.8}$	$0.63^{+0.17}_{-0.15}$	6.93	1.18	$\gtrsim 22^S$	$\gtrsim 1.14$	<3.41	
25	034654.2+675902		6.8	$27.7^{+8.5}_{-6.5}$	< 0.66	3.99	0.68	$\gtrsim 20$	$\gtrsim 0.10$	<2.64	
26	034657.7+680616	R9	1.0	$1204.9^{+37.4}_{-35.7}$	$0.79^{+0.05}_{-0.05}$	41.34	8.96	$\gtrsim 22^S$	$\gtrsim 2.02$	10.50	
27	034702.2+680234		3.4	$114.2^{+13.6}_{-11.7}$	$0.94^{+0.22}_{-0.20}$	8.32	1.42	$\gtrsim 20$	$\gtrsim 0.45$	<3.32	
28	034704.5+680904		3.6	$89.5^{+12.8}_{-10.9}$	$1.05^{+0.30}_{-0.27}$	6.39	1.09	$\gtrsim 24^S$	$\gtrsim 1.91$	<2.50	
29	034704.8+680515		1.6	$42.0^{+10.2}_{-8.3}$	$0.20^{+0.18}_{-0.13}$	2.30	0.39	18.5	–0.74	<3.54	HII Region? ($1.''3$)
30	034719.2+681129		6.4	$198.8^{+18.5}_{-16.7}$	$0.28^{+0.08}_{-0.07}$	9.85	5.66	21.4^S	1.13	<3.07	($1.''0$)
31	034723.3+680857		4.5	$267.2^{+20.1}_{-18.3}$	$0.34^{+0.07}_{-0.06}$	6.90	7.71	$\gtrsim 20$	$\gtrsim 0.42$	<2.73	
32	034805.9+680138		8.3	$25.0^{+9.3}_{-7.3}$	< 0.77	2.38	0.41	$\gtrsim 20$	$\gtrsim -0.12$	<3.13	
33	034807.4+680451	R10	7.4	$202.8^{+18.3}_{-16.5}$	$0.67^{+0.13}_{-0.12}$	10.05	2.81	$\gtrsim 20$	$\gtrsim 0.66$	4.70	
34	034818.3+680205		9.1	$67.2^{+11.8}_{-9.9}$	$0.74^{+0.28}_{-0.24}$	7.62	1.30	$\gtrsim 20$	$\gtrsim 0.38$	<2.74	
35	034826.4+680815		9.4	$22.5^{+9.6}_{-7.6}$	$0.55^{+0.60}_{-0.45}$	2.87	0.49	$\gtrsim 20$	$\gtrsim -0.04$	<2.48	

NOTE. — Column 1: ID number. Sources denoted by a "*" are not thought to be intrinsic to IC 342. Column 2: Source name given as XMMU JHHMMSS.S+DDMMSS. Sources denoted by a † were rejected by *emldetect* for no obvious reason (see §2). Column 3: Other names. R# and A# indicate the *ROSAT* and *ASCA* source numbers assigned by BCT93 and O98, respectively. Column 4: Off-axis angle in units of arcminutes. Column 5: Background-subtracted 0.3–10 keV counts, summed over all of the EPIC instruments (pn+MOS1+MOS2). Aperture photometry was performed using extraction radii ranging in radius from ≈17–68″, depending on off-axis angle and the relative brightness of the source compared to the local background (see §2). The errors for the source and background counts were computed following the method of Gehrels (1986) and were then combined following the "numerical method" described in §1.7.3 of Lyons (1991). Column 6: Band ratios, defined as the ratio of counts between the hard and soft bands. The quoted band ratios have been corrected for differential vignetting between the hard band and soft band using the appropriate exposure maps. Errors for this quantity are calculated following the "numerical method" described in §1.7.3 of Lyons (1991). Column 7: Observed, aperture-corrected 0.5–10 keV fluxes in units of 10^{-14} erg cm^{-2} s^{-1} from the best-fit models to the *XMM-Newton* spectra (see Table 2). For faint sources (< 150 counts), fluxes were calculated assuming an average power-law spectrum with $N_H = 3.4 \times 10^{21}$ cm^{-2} and a photon index of $\Gamma = 1.63$ as determined from the stacked spectrum of the faint sources. Column 8: Absorption-corrected 0.5–10 keV luminosities in units of 10^{38} erg s^{-1} from the best-fit models to the *XMM-Newton* spectra. Column 9: R magnitude as derived from the Saha et al. (2002) r' image (indicated by an "S") or USNOB1. The magnitude lower limits were estimated based on the faintest detectable sources within the vicinity of the X-ray source. Column 10: X-ray-to-optical flux ratio using columns 7 and 9 such that $\log(F_X/F_O)=\log(F_X)+5.5+R/2.5$. Column 11: Observed, aperture-corrected 0.5–2 keV fluxes in units of 10^{-14} erg cm^{-2} s^{-1} from the *ROSAT* HRI derived using XIMAGE and PIMMS. The adopted spectral models were identical to those assumed in Column 5. Column 13: Possible optical ID and additional comments. Saha and USNOB1 offsets are provided in parentheses for sources with optical counterparts.

(Proposal IDs 00011, 10946, 11220, 11229), and from extrapolation of the medium-deep *XMM-Newton* $\log N$–$\log S$ of Baldi et al. (2002, i.e., ≈ 60–100 sources per deg^2 down to a limiting 0.5–10 keV flux of $\approx 1 \times 10^{-14}$ erg cm^{-2} s^{-1}), we would expect ∼ 7–12 foreground or background sources within a 12′ radius of IC 342. Given that we are able to identify four of our 35 sources with foreground stars (sources 2, 11, 15, and 20), we suspect that the majority of the remaining 31 X-ray sources are associated with IC 342 based on their large X-ray-to-optical flux ratios; half have $\log(F_X/F_O) \gtrsim 0.5$, and all but the nucleus have $\log(F_X/F_O) \gtrsim -0.5$. A comparison of the X-ray-to-optical flux ratios of these sources with Figure 1 of Maccacaro et al. (1988, after accounting for average X-ray and optical band differences) suggests these sources are inconsistent with X-ray emission from all normal stars and even some AGN (the most likely foreground and background contaminants, respectively), but they are fully consistent with X-ray binaries in IC 342. Additionally, sources that are significantly brighter than our limiting X-ray flux, and are therefore rarer, are even more likely to be associated with IC 342. For instance, there is a $\lesssim 0.1\%$ chance that any of the four sources brighter than $\approx 5 \times 10^{-13}$ erg cm^{-2} s^{-1} are foreground or background X-ray sources.

Point-source spectra were extracted using the apertures described above. Event PI values and photon energies were determined using the latest gain files appropriate for the observation. The X-ray spectra were analyzed using `XSPEC` (Arnaud 1996). Unless stated otherwise, spectral parameter errors are for 90% confidence assuming one parameter of interest ($\Delta\chi^2 = 2.7$). The X-ray fluxes and absorption-corrected luminosities for all 35 sources were calculated from spectral fitting using `XSPEC`. None of the sources was affected by pile-up. For faint sources (< 150 counts) thought to be intrinsic to IC 342 (i.e., not obvious foreground stars), fluxes were calculated assuming an average absorbed power-law spectrum with $N_{\rm H} = (3.4^{+0.9}_{-0.7}) \times 10^{21}$ cm^{-2} and a photon index of $\Gamma = 1.63^{+0.13}_{-0.14}$, as determined from the stacked spectrum of the faint sources. Fluxes for the two faint foreground stars (sources 2 and 15) were calculated assuming the spectrum of source 11 (see Table 2). Note that if a faint source's spectrum deviates substantially from these average values, then the flux and absorption-corrected luminosity of the source may change as well.

3. IC 342 X-RAY PROPERTIES

The 31 point sources plausibly associated with IC 342 span over two orders of magnitude in X-ray luminosity and display a diverse range of spectral properties, as implied from the band ratios listed in Table 1 (*BR* ~ 0.1–3.4). The 0.5–10 keV X-ray luminosity function (XLF) of the sources is relatively flat down to $L_{\rm X} \sim 4 \times 10^{37}$ erg s^{-1} with a slope of 0.5 ± 0.1, as determined from maximum likelihood fitting of the differential XLF. At luminosities fainter than this limit, incompleteness due to the sensitivity limit and absorption bias against soft sources makes the XLF slope uncertain. Somewhat surprisingly, we detect little diffuse X-ray emission (only a compact region around the nucleus; see §3.1). In estimating the amount of diffuse emission, we only used the combined MOS1+MOS2 0.3–2.0 keV image for simplicity. We extracted a total of 124 ± 48 counts within a 5′ radius aperture around the nucleus, using a vignetting-corrected 5–10′ background annulus and masking out point sources using their 99% encircled-energy radius apertures. Assuming this emission would have an absorbed thermal plasma spectrum with a temperature of 0.5 keV (1 keV) and column density of $N_{\rm H} = 6 \times 10^{21}$ cm^{-2} (see §3.3), our 3σ upper limit corresponds to a flux density of $< 8.4 \times 10^{-15}$ erg cm^{-2} s^{-1} arcmin^{-2} ($< 9.9 \times 10^{-16}$ erg cm^{-2} s^{-1} arcmin^{-2}) and an absorption-corrected 0.5–2.0 keV luminosity of $L_{\rm X} < 5.6 \times 10^{39}$ erg s^{-1} ($L_{\rm X} < 3.0 \times 10^{38}$ erg s^{-1}).

In addition to these global properties, the *XMM-Newton* observation provides constraints on the spatial, spectral, and temporal properties of the X-ray point-source population as detailed below.

3.1. *Spatial Extent of the Nuclear Source XMMU J034648.8+680546 (IC 342 X-3)*

This *XMM-Newton* observation offers an order of magnitude improvement compared to the high-resolution *ROSAT* HRI observations in the number of counts collected from the nucleus of IC 342, allowing us to improve measurements of the nuclear spatial extent reported by BCT93. The nuclear source appears to be azimuthally symmetric in the raw images out to ∼40″, so we extracted soft and hard-band counts from it in 1.″1 (1 MOS pixel) annular bins using the combined MOS1+MOS2 image; the spatial resolution of the PN is $\gtrsim 1.5\times$ worse (*XMM-Newton* Users' Handbook §3.2.1.1) and is therefore not very useful for this purpose. We also generated images of the MOS1+MOS2 PSF using the `SAS` calibration tool `calview`. Counts from these images were then extracted in an identical manner to the data and normalized by the innermost nuclear annulus. The resulting radial surface-brightness distributions and 1σ errors for the data are shown in Figure 3.

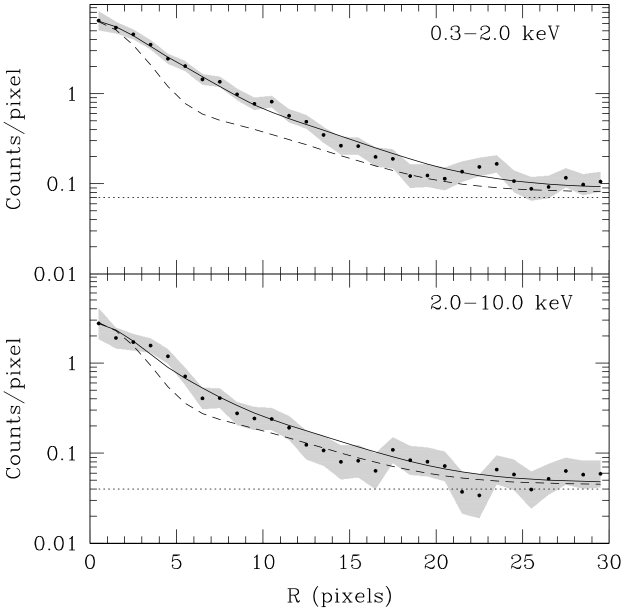

FIG. 3.— The soft and hard-band MOS1+MOS2 radial profiles (small filled circles) of the IC 342 nucleus, compared to our simple model (solid curves) and the *XMM–Newton* PSF (dashed curves) calculated at 1.5 keV and 6 keV, respectively; see §3.1 for details. The average background has been added to both the model and the PSF. The shaded regions indicate the 1σ deviation of the measured profile. Deviations from the PSF, particularly in the soft band, can be seen out to radii of ≈20 and ≈10 pixels, at which point the 0.07 counts pixel^{-1} soft-band and 0.04 counts pixel^{-1} hard-band backgrounds begin to dominate (dotted lines), respectively. A MOS pixel is equivalent to 1.″1.

The surface-brightness distribution of the nucleus lies above the background out to radii of ∼15–20 pixels (∼ 16–22″) and is clearly extended compared to the PSF model. The accuracy of the MOS PSF model from `calview` was verified using source 26 (1′ from the nucleus); deviations between this source and the PSF were much smaller than those seen in Figure 3 and were consistent with source statistics. The fact that the fraction of extended emission is larger in the soft band, even though the imaging quality is similar in both bands, further supports the reality of the extent. An emission model consisting of both a point source and a uniform disk with an ≈ 8″ (128 pc) radius convolved with the instrument PSF represents the surface-brightness distribution well, although there is clearly still some residual scatter due to possible clumping or patchy absorption. This is especially noticeable in the hard band where individual point sources are more likely to dominate the emission. The relative contributions from the extended disk component are ≈ 55% and ≈ 35% in the soft and hard bands, respectively, in crude agreement with the BCT93 soft-band values (9″ radius, 44%). The relative softness of the extended emission is consistent with its expected physical origin as supernova-heated hot gas (see also §3.3.3 for X-ray spectral details). Moreover, the extent of the X-ray disk emission mirrors the surface brightness enhancements seen at optical-to-radio wavelengths (≈ 10–15″; e.g., Böker et al. 1997; Buta & McCall 1999; Schinnerer et al. 2003) that are attributed to a starburst ring, further strengthening our conclusions.

3.2. *X-ray Timing Analysis*

3.2.1. *Short-Term Variability*

Although the *XMM-Newton* observation of IC 342 was short, we do have adequate statistics to evaluate the short-term timing characteristics of some of the off-nuclear sources. To examine objectively the existence of any significant variations in the count rate, we used the Kolmogorov-Smirnov (KS) statistic on the unbinned data to test the null hypothesis that each source plus background rate was constant over the duration of the exposure. None of the sources varied at the $> 90\%$ confidence level.

3.2.2. *Long-Term Variability*

Comparison of the *XMM-Newton* observation with the 19 ks *ROSAT* HRI observation on 1991 February 13–16 allows us to constrain the soft-band long-term variability of the entire IC 342 X-ray source population, while comparison with the 38 ks *ASCA* observation on 1993 September 19 and the 276 ks *ASCA* observation on 2000 February 24–March 1 allows us to constrain the full-band variability for X-1, X-2, and X-3. The hard-band variability will be discussed in §3.3 in the context of our X-ray spectral analyses.

To measure the soft-band variability, we extracted the HRI counts at the position of each source using the `XIMAGE` software package, which corrects for vignetting and aperture losses. For detections, we used the values reported in BCT93, and for 3σ upper limits we used the *sosta* algorithm. The HRI count rates were converted to 0.5–2 keV fluxes using PIMMS (column 10 of Table 1). The PIMMS input spectral model was set to the best-fit model found from our `XSPEC` spectral analyses in §3.3. We found that five sources were variable in the soft band over the 10-year period: XMMU J034556.0+680455 and XMMU J034646.0+680946 faded by a factor of ≈6 and ≈3.3. compared to the *ROSAT* observation, respectively; XMMU J034719.2+681129 and XMMU J034723.3+680857 brightened by at least factors of 1.5 and 1.4 compared to their *ROSAT* upper limits, respectively; and finally J034541.4+680241 (*ROSAT* source 2; BCT93) was not detected by our *XMM-Newton* observation at all, indicating a decrease of at least a factor of 5. Given the poor HRI statistics for this latter source, however, it may have been spurious, although strong variability or extreme X-ray spectral properties (i.e., a very soft spectrum) cannot be ruled out.

3.3. *X-ray Spectral Analysis*

For each source, we extracted the spectra and response matrices for each CCD camera separately and fit all three spectra with the same model in `XSPEC`. We initially fitted the spectra with absorbed power-law models.[5] The spectral properties of the 23 sources with fewer than 150 full-band counts are not well constrained and have been fitted only with a mean spectrum as given in §2 to derive X-ray fluxes and luminosities. The 12 sources with more than 150 full-band counts all had adequate photon statistics for individual fits, although $\gtrsim 1000$ counts were typically necessary to rule out competing spectral models clearly. The best-fit spectral parameters for these 12 sources are given in Table 2. All of the sources thought to be intrinsic to IC 342 exhibited spectral cutoffs below ~ 1 keV that are best fit with column densities equal to or larger than the Galactic value (see §1), consistent with these off-nuclear X-ray sources being located in star-forming regions and spiral arms within IC 342. We discuss our results for the four brightest X-ray sources in IC 342 with > 1000 counts below.

3.3.1. *XMMU J034556.0+680455 (IC 342 X-1)*

IC 342 X-1 is the brightest source in IC 342 and was recently found to be coincident with a supernova remnant (Roberts et al. 2003). X-1 has been extensively studied by *ASCA*, as it is considered to be one of the best examples of a massive ($\gtrsim 10 M_{\odot}$) black-hole binary. O98 found this source in a luminous high state in 1993, with a spectrum best-fitted by an absorbed multi-color disk model (*diskbb* model in XSPEC; Mitsuda et al. 1984) arising from an optically thick standard accretion disk around a black hole. The best-fit absorbed *diskbb* parameters were $N_{\rm H} = (4.7 \pm 0.3) \times 10^{21}$ cm^{-2} and $T_{\rm in} = 1.77 \pm 0.05$ keV, resulting in a 0.5–10 keV flux of $F_{0.5\text{–}10\ {\rm keV}} \approx 1.0 \times 10^{-11}$ erg cm^{-2} s^{-1}. When it was revisited in 2000, K01 found the flux ($F_{0.5\text{–}10\ {\rm keV}} \approx 3.1 \times 10^{-12}$ erg cm^{-2} s^{-1}) and spectrum of this source had changed dramatically, and it was best fit by an absorbed power-law model with $N_{\rm H} = (6.4 \pm 0.7) \times 10^{21}$ cm^{-2} and $\Gamma = 1.73 \pm 0.06$. An ionized Fe-K edge at 8.4 ± 0.3 keV with an optical depth of 0.9 ± 0.5 was also seen. K01 attributed this spectral change to be a transition between a high/soft state and a low/hard state, as is observed in many Galactic and Magellanic black-hole binary systems. Kubota et al. (2002, hereafter K02) re-examined the 2000 *ASCA* data, finding that the spectrum deviates from a power-law shape such that there appears to be significant softening above 5 keV. They proposed that the spectrum was not indicative of a low-hard state, but rather of an anomalous very high (VH) state as observed in some Galactic black-hole binaries, which was adequately fit by a strongly Comptonized optically thick accretion disk with $T_{\rm in} = 1.1 \pm 0.3$ keV and $\Gamma^{\rm th} = 2.2 \pm 0.4$. We note that the *ASCA* $\approx 2\overset{\prime}{.}5$ radius beam used to study X-1 (compare with Figure 1 of O98) would have also included sources 6, 9, and 11 from Table 1, contaminating the *ASCA* source by ≈ 19% based on the relative *XMM–Newton* source fluxes.

To compare with the *ASCA* spectral fits, we fitted both an absorbed *diskbb* model and an absorbed power law to the X-ray spectrum. The best-fit parameters for the absorbed *diskbb* model were $T_{\rm in} = 1.93^{+0.14}_{-0.13}$ keV and $N_{\rm H} = (3.5^{+0.3}_{-0.3}) \times 10^{21}$ cm^{-2} ($\chi^2 = 206.9$ for 193 degrees of freedom), while those for the absorbed power law were $\Gamma = 1.68^{+0.09}_{-0.08}$ and $N_{\rm H} = (6.0^{+0.5}_{-0.5}) \times 10^{21}$ cm^{-2} ($\chi^2 = 166.0$ for 193 degrees of freedom). Although the *diskbb* fit is formally acceptable, there are systematic residuals at the softest and hardest energies, and hence the power-law model appears to offer a superior fit to the data (see the X-1 residuals in Figure 4). The flux of the source is found to be $F_{0.5\text{–}10\ {\rm keV}} \approx 2.15 \times 10^{-12}$ erg cm^{-2} s^{-1} The best-fit parameters from the power-law model are consistent with those obtained during the 2000 *ASCA* observation, suggesting that little changed spectrally in the ≈27.5 months between the latest *ASCA* observation and our *XMM-Newton* observation. The *XMM-Newton* flux, on the other hand, is ≈ 30% lower than the 2000 *ASCA* measurement. This is a bit larger than the source confusion estimate made above (accounting for slight bandpass differences), but the difference is only marginally significant. Thus we conclude that X-1 has remained relatively constant over the ≈ 2 yrs between the latest *ASCA* and *XMM–Newton* observations and is therefore likely to be in a VH state similar to the one reported by K02.

---

[5] In most cases, a *mekal* thermal plasma model (Mewe et al. 1985) was equally acceptable.

TABLE 2. X-RAY SPECTRAL ANALYSIS RESULTS

(1) ID	(2) Best-fit Model	(3) $N_{\rm H}$	(4) $\Gamma/kT/T_{\rm in}$	(5) χ^2/DOF	(6) Comments
7	P	$6.0^{+0.5}_{-0.5}$	$1.68^{+0.09}_{-0.08}$	166.0/193	BB model also acceptable, but shows systematic residuals
13	BB	$15.3^{+1.9}_{-1.8}$	$2.17^{+0.25}_{-0.12}$	113.0/108	P model shows somewhat worse residuals
19	P	$4.6^{+1.8}_{-1.4}$	$1.84^{+0.39}_{-0.16}$	17.6/16	
21	T+P	$6.4^{+0.7}_{-1.0}$	$kT = 0.30^{+0.33}_{-0.07}/\Gamma = 2.52^{+0.15}_{-0.18}$	94.4/97	One-component models are not acceptable, $Z = 6.39(> 1.45)Z_{\odot}$
26	BB	$2.0^{+0.9}_{-0.7}$	$1.46^{+0.21}_{-0.17}$	45.1/52	P and T models also acceptable, but show some systematic residuals
ID	Best-fit Model	$N_{\rm H}$	$\Gamma/kT/T_{\rm in}$	*cstat*/DOF	Comments
6	P	$6.7^{+1.1}_{-2.5}$	$1.77^{+0.16}_{-0.16}$	1375.5/3233†	T model also acceptable, but shows worse residuals
9	P	$5.2^{+0.8}_{-1.0}$	$1.82^{+0.16}_{-0.14}$	1255.7/3233†	
11*	T	$6.2^{+0.7}_{-0.6}$	$0.17^{+0.03}_{-0.01}$	870.6/3233†	Soft X-ray spectrum, consistent with star ID
20*	T	$2.8^{+3.6}_{-1.9}$	$0.25^{+0.04}_{-0.08}$	706.2/3233†	Soft X-ray spectrum, consistent with faint star ID, $Z = 0.28^{+0.38}_{-0.13}Z_{\odot}$
30	P	$6.9^{+4.3}_{-1.6}$	$3.14^{+1.54}_{-0.18}$	842.8/3233†	T and BB models also acceptable.
31	P	$8.6^{+0.8}_{-2.7}$	$3.79^{+0.41}_{-0.76}$	969.8/3233†	T and BB models also acceptable.
33	P	$4.7^{+0.8}_{-0.7}$	$2.17^{+0.19}_{-0.18}$	1046.1/3233†	

NOTE. — Col. 1: ID number. Sources denoted by a "*" are not thought to be intrinsic to IC 342. Column 2: Best-fit spectral model from XSPEC for bright sources (> 150 counts). For sources with fewer than 400 total counts, the Cash statistic (Cash 1979) was used instead of χ^2. All models were fit with a *wabs* absorption component. A "P" indicates a power-law component, a "T" indicates a *mekal* thermal-plasma component, and a "BB" indicates a multi-color disk component. Note that the Galactic column toward IC 342 is $N_{\rm H} = 3 \times 10^{21}$ cm^{-2} (Stark et al. 1992). Column 3: Neutral hydrogen absorption column density in units of 10^{21} cm^{-2} as determined from the best-fit models to the *XMM-Newton* spectra. Also listed are the 90% confidence errors calculated for one parameter of interest ($\Delta\chi^2 = 2.7$). Column 4: Power-law photon index Γ, thermal-plasma temperature kT (keV), or multi-color disk inner temperature $T_{\rm in}$ as determined from the best-fit models to the *XMM-Newton* spectra. Also listed are the 90% confidence errors calculated for one parameter of interest ($\Delta\chi^2 = 2.7$). Column 5: χ^2 and degrees of freedom. Sources denoted by a "†" were fit with the Cash statistic on the unbinned data, in which case the "cstat" value and degrees of freedom are listed. Column 6: Comments.

If X-1 truly is in a VH state, and this state has remained roughly constant for ≈ 2 yrs, then it marks the longest period over which a VH state has been observed. For comparison, this would be $\approx 10\times$ longer than has been observed in GX 339-4, a Galactic binary which went into a VH state for $\approx$3 months (M. Nowak 2003, private communication). Given the limited amount of information regarding the VH state in general, the longevity of the VH state observed in X-1 is plausibly consistent with current understanding of this state. Another possibility is that both the 2000 *ASCA* and 2002 *XMM-Newton* observations caught X-1 in a VH state, but it varied out of the VH state in between. GRS 1915+105, for instance, is known to vary in and out of the VH state frequently and has a non-negligible duty cycle in the VH state (e.g., Belloni et al. 2000).

3.3.2. *XMMU J034616.0+681115 (IC 342 X-2)*

IC 342 X-2 is the second brightest source in IC 342 and also has been extensively studied by *ASCA*. In contrast to X-1, this source was in a low state in 1993 with $F_{0.5\text{–}10\ {\rm keV}} \approx 4.1 \times 10^{-12}$ erg cm^{-2} s^{-1}. Its X-ray spectrum was acceptably fit by either an absorbed power-law or *diskbb* model (O98, K01). The best-fit absorbed power-law parameters were $N_{\rm H} = (14.3 \pm 1.6) \times 10^{21}$ cm^{-2} and a photon index of $\Gamma = 1.39 \pm 0.10$ keV. In 2000, K01 found that the flux of this source had nearly doubled to $F_{0.5\text{–}10\ {\rm keV}} \approx 7.2 \times 10^{-12}$ erg cm^{-2} s^{-1}, and its spectrum was best fit by an absorbed *diskbb* model with $N_{\rm H} = (18.0 \pm 8.0) \times 10^{21}$ cm^{-2} and $T_{\rm in} = 1.62 \pm 0.04$ keV. K01 attributed this to be a spectral transition between a low/hard state and a high/soft state. As with X-1, we note that the *ASCA* $\approx 3\farcm0$ radius beam used to study X-2 would have also included source 12 and possibly source 20 (compare with Figure 1b of K01). The contamination from these sources to the *ASCA* source, however, is only $\approx$ 3–10% based on the relative *XMM–Newton* source fluxes (and should be even less after the strong variability seen from X-2 is accounted for; see below).

Based on the *ASCA* spectral fits, we fitted both absorbed *diskbb* and power-law models to the X-ray spectrum of X-2. We note that X-2 lies along a chip gap in the MOS2 detector, resulting in a 50% loss of counts with that device. The best-fit parameters for the absorbed *diskbb* model were $T_{\rm in} = 2.17^{+0.25}_{-0.12}$ keV and $N_{\rm H} = (15.3^{+1.9}_{-1.8}) \times 10^{21}$ cm^{-2} ($\chi^2 = 113.0$ for 108 degrees of freedom), while those for the absorbed power-law model were $\Gamma = 1.81 \pm 0.18$ and $N_{\rm H} = (22.5^{+3.3}_{-2.9}) \times 10^{21}$ cm^{-2} ($\chi^2 = 127.3$ for 108 degrees of freedom). Both models provide acceptable fits to the data, although the residuals of the *diskbb* model exhibit fewer systematic deviations (see Figure 4). The best-fit parameters are different from those obtained during either *ASCA* observation, demonstrating that X-2 has undergone further spectral variability. In addition, the *XMM-Newton* flux has dropped by factors of $\sim$1.7 and $\sim$3 compared with the *ASCA* results of 1993 and 2000. Thus although this state is spectrally intermediate between the 1993 and 2000 states, it is the lowest flux state exhibited by X-2 to date. It is interesting that this new low/hard state is better fit by the *diskbb* model than a power-law model, as this indicates that X-2 still has some spectral curvature. This curvature is in the opposite sense to that expected from a soft thermal component with a hard tail (i.e., the standard for X-ray binaries in their high state). The column density observed toward this source, however, is a factor of $\approx$2–3 higher than seen from any of the other sources, suggesting that X-2 has significant local absorption. It is therefore possible that the apparent curvature is due to complex absorption near the source, which is also often detected in luminous Galactic X-ray binaries.

3.3.3. *XMMU J034648.8+680546 (IC 342 X-3)*

IC 342 X-3 is coincident with the nucleus and was clearly detected by both the *ROSAT* HRI and *ASCA*. The spectral properties of X-3 from the 1993 *ASCA* observation are discussed briefly in O98, who found that the source was best fitted by an absorbed power law with $\Gamma = 2.1 \pm 0.2$ and fixed $N_{\rm H} = 3.0 \times 10^{21}$ cm^{-2}. Again, we note that the *ASCA* $\approx 3\farcm0$ ra-

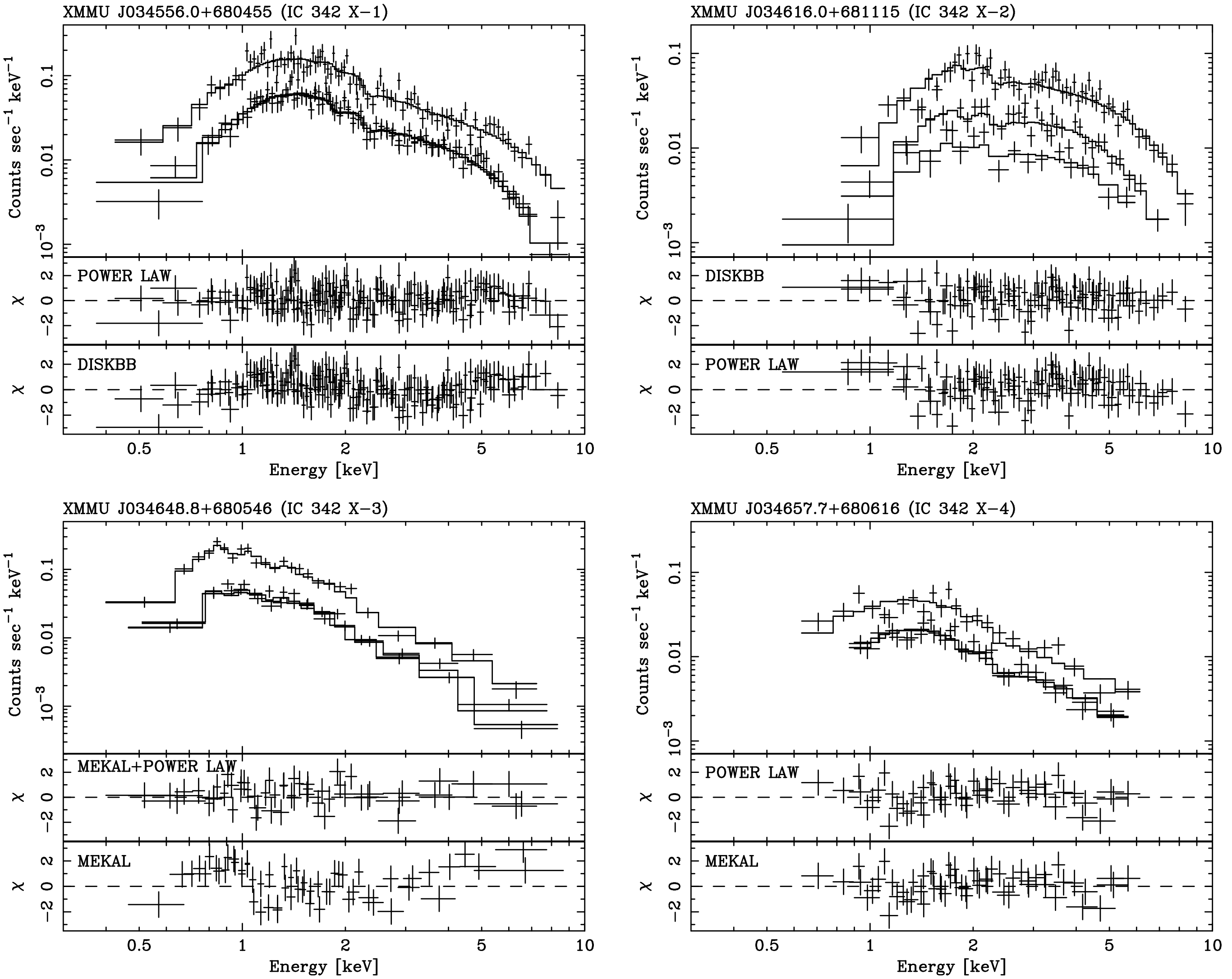

FIG. 4.— X-ray spectra of the four brightest X-ray sources in IC 342. The upper panel of each plot shows the PN, MOS1, and MOS2 spectra and best-fit models (see §3.3 for details). The lower two panels show the residuals of the fits measured in units of σ for the best-fit model (middle) and the next most likely model (bottom).

dius beam used to study X-3 would have also included sources 19, 24, 26, and 29 (compare with Figure 1 of O98). The contamination from these sources to the *ASCA* source is $\approx$ 44% based on the relative *XMM–Newton* source fluxes.

We initially fitted both single absorbed power-law and thermal-plasma models to the X-ray spectrum of the nucleus. Both fits were unacceptable, with the absorbed power-law model giving $\Gamma = 2.67$ and $N_{\rm H} = 4.0 \times 10^{21}$ cm^{-2} ($\chi^2 = 180.4$ for 101 degrees of freedom), and the absorbed *mekal* model giving $kT = 2.14$ keV, $Z = 0.02 Z_{\odot}$, and $N_{\rm H} = 2.4 \times 10^{21}$ cm^{-2} ($\chi^2 = 214.9$ for 100 degrees of freedom). Neither model acceptably fits the continuum shape or the apparent Fe L-shell emission complexes visible at $\approx$0.8 keV and $\approx$1.0 keV (see Figure 4). The presence of Fe L-shell emission at these two energies suggests that a large fraction of the emission is likely to be thermal in origin. In §3.1 we were able to separate spatially X-3 into point-like and extended components. Thus we should expect that the spectrum of X-3 might be complex, consisting of perhaps two or more components. We therefore modeled the spectrum with an absorbed *mekal*+power-law model. This model provides a significant improvement over the single-component models ($\chi^2 = 94.4$ for 96 degrees of freedom), with best-fit values of $kT = 0.30^{+0.33}_{-0.07}$ keV, $\Gamma = 2.52^{+0.15}_{-0.18}$, $Z = 6.39 (> 1.45) Z_{\odot}$, and $N_{\rm H} = (6.8^{+1.6}_{-1.5}) \times 10^{21}$ cm^{-2}. An absorbed *mekal*+*mekal* model with a single metallicity also provides an acceptable fit to the data ($\chi^2 = 97.9$ for 96 degrees of freedom), with best-fit values of $kT_1 = 0.50^{+0.12}_{-0.22}$ keV, $kT_2 = 4.02^{+1.89}_{-1.30}$ keV, $Z = 0.12^{+0.08}_{-0.07} Z_{\odot}$, and $N_{\rm H} = (5.0^{+2.2}_{-1.1}) \times 10^{21}$ cm^{-2}. However, the best-fit abundance for this second model is low compared to the optically derived value of $\approx 3Z_{\odot}$ (Diaz & Tosi 1986; Vila-Costas & Edmunds 1992). Fixing the absorbed *mekal*+*mekal* model abundance at $3Z_{\odot}$ (or even $Z_{\odot}$) results in an unacceptable fit with $\chi^2 = 169.9$ ($\chi^2 = 120.5$) for 97 degrees of freedom. The absorbed *mekal*+power-law model on the other hand provides a consistent measure of the nuclear abundance.

The relative contribution of the mekal component to the total absorbed flux of X-3 is 45% and 1% in the soft and hard bands, respectively. The soft-band fraction is in basic agreement with the physical picture found from our spatial analysis (§3.1), suggesting that the soft thermal plasma component is likely to be spatially extended and of a starburst origin. The complete domination of the power-law component above 2 keV, coupled with the fact that we still find significant amount extended emission in this band, suggests that the hard component is probably complex and may be due to an unknown number of circumnuclear X-ray binaries.[6] The absorption-corrected 0.5–10.0 keV luminosity of the extended nuclear component is $L_{\rm X} \approx 2.1 \times 10^{39}$ erg s^{-1}), which is comparable to or larger than our constraint on extended emission from the rest of IC 342.

3.3.4. *XMMU J034657.7+680616 (IC 342 X-4)*

IC 342 X-4 is a bright source located $\approx 1\overset{\prime}{.}0$ from the nucleus, which was only resolved by the *ROSAT* HRI observation (*ROSAT* source 9; BCT93). The source was presumably detected by *ASCA* as well but was blended together with the nucleus in those observations, contributing ≈ 31% based on the relative *XMM–Newton* source fluxes. We initially fitted X-4 with an absorbed power-law model, obtaining an acceptable fit with best-fit parameters of $N_{\rm H} = (4.4^{+1.4}_{-1.0}) \times 10^{21}$ cm^{-2} and $\Gamma = 1.80^{+0.20}_{-0.09}$ ($\chi^2 = 51.8$ for 52 degrees of freedom). We found that *diskbb* and *mekal* models provided equally acceptable fits. However, while the *diskbb* model fit the continuum shape best (see the X-4 residuals in Figure 4), the best-fit absorption column value lies just below Galactic. In the case of the *mekal* model, the high temperature would imply that X-4 must be a young supernova, although it clearly lacks the long-term variability or high equivalent-width X-ray emission lines characteristic of such sources. Thus it seems that the power-law model is the most physically appropriate model. If X-4 is a single X-ray binary, then its low photon index may indicate that it is in a low/hard state; however, its spectral ambiguity leaves room for several other possibilities as well.

4. CONCLUSIONS

Our *XMM–Newton* observation has tripled the number of known X-ray point sources in IC 342 and has provided a number of new constraints on the X-ray properties of both the point-source population and any potential diffuse emission.

- We find a relatively flat XLF slope of 0.5±0.1 for IC 342, which is comparable to those found for actively star-forming galaxies such as M82 and the Antennae and is inconsistent with those of quiescent spiral galaxies (e.g., Kilgard et al. 2002; Colbert et al. 2003). This implies that IC 342 may have played host to a significant amount ($\gtrsim 0.5\ M_\odot$ yr^{-1}) of recent star-formation activity. However, our upper limit on diffuse X-ray emission associated with hot gas ($L_{\rm X} < 5.6 \times 10^{39}$ erg s^{-1} for a 0.5 keV thermal plasma), and its infrared luminosity of $L_{60\ \mu m} = 9 \times 10^{42}$ erg s^{-1} (Shapley et al. 2001), are more typical of other Sab galaxies such as M58 or M94 (e.g., Eracleous et al. 2002) rather than luminous starbursts (e.g., Read et al. 1997). Thus IC 342 appears to have the X-ray binary population of a starburst, but lacks the hot gas and luminous infrared emission that typically accompanies vigorous star formation. This suggests that the mode of star formation in IC 342 is probably quite different from that of archetypal starburst sources.

- We find no evidence for short-term variability among the X-ray sources in this short observation. We do find long-term variability between this observation and the 1991 *ROSAT* and 1993/2000 *ASCA* observations for five sources.

- We find X-1 to be in a state identical to the one observed by *ASCA* in 2000, after correcting the *ASCA* measurement for source contamination. If X-1 is in a VH state as contended by K02, and it has remained in this state between 2000 and 2002, then it would be the longest duration VH-state binary ever observed. Alternatively, it might be possible that both the 2000 *ASCA* and 2002 *XMM-Newton* observations caught X-1 in a VH state by chance, but that it has varied out of the VH state in between.

- We find X-2 has decreased in flux by factors of ∼1.7 and ∼3 compared to its states observed by *ASCA* in 1993 and 2000, respectively, while its spectrum is intermediate between the low/hard 1993 state and the high/soft 2000 state. This is the lowest luminosity state observed for X-2 to date.

- We have confirmed that a large fraction (≈55% and ≈35% in the 0.3–2.0 keV and 2.0–10.0 keV bands, respectively) of the X-ray emission coincident with nucleus of IC 342 is associated with an extended, relatively uniform disk approximately $8''$ in radius. The spectrum of the nucleus is best fit by an absorbed two-component model consisting of a thermal plasma with a temperature of $kT \approx 0.3$ and a power law with a photon index of $\Gamma \approx 2.53$. The relative fluxes of the two spectral components suggest that the nucleus is complex, with a soft extended component contributing ≈50% of the total luminosity.

Because of their relative distance and luminosity, the X-ray binaries in IC 342 provide an excellent laboratory to advance our knowledge of ultraluminous X-ray sources even further. For instance, a higher signal-to-noise spectrum of X-1 with *XMM-Newton* or *Constellation-X* might provide stronger constraints on its nature, especially regarding the origin of the spectral softening above 4 keV and an apparent spectrum bump around 1.5 keV. Uniform temporal monitoring of X-1, X-2, and X-3 could provide more information about the frequency and amplitude of spectral transitions, which would help place stronger limits on their black hole masses. Finally, higher resolution X-ray imaging of the nucleus with *Chandra* would allow a decoupling of the extended and point-like emission with the two spectral components.

We thank I. Lehmann, M. Nowak, and C. Vignali for helpful discussions, and R. Buta and A. Saha for use of their optical images. We gratefully acknowledge the financial support of NASA awards NAG5-10089 (FEB), NAG5-9940 (BL, WNB), and LTSA NAG5-13035.

[6] Another possible origin for the point-like fraction of the point-like emission is from a low-luminosity active nucleus, although there is no evidence for one from past studies of the nuclear region.

REFERENCES

Arnaud, K. A. 1996, in ASP Conf. Ser. 101: Astronomical Data Analysis Software and Systems V, vol. 5, 17–20

Baldi, A., Molendi, S., Comastri, A., Fiore, F., Matt, G., & Vignali, C. 2002, ApJ, 564, 190

Belloni, T., Klein-Wolt, M., Méndez, M., van der Klis, M., & van Paradijs, J. 2000, A&A, 355, 271

Böker, T., Forster-Schreiber, N. M., & Genzel, R. 1997, AJ, 114, 1883

Bregman, J. N., Cox, C. V., & Tomisaka, K. 1993, ApJ, 415, L79, (BCT93)

Buta, R. J. & McCall, M. L. 1999, ApJS, 124, 33

Cash, W. 1979, ApJ, 228, 939

Colbert, E., Heckman, T., Ptak, A., & Strickland, D. 2003, ApJ, submitted (astro-ph/0305476)

Crosthwaite, L. P., Turner, J. L., & Ho, P. T. P. 2000, AJ, 119, 1720

Diaz, A. I. & Tosi, M. 1986, A&A, 158, 60

Ebeling, H., White, D., & Rangarajan, F. V. N. 2003, MNRAS, 0, submitted

Eracleous, M., Shields, J. C., Chartas, G., & Moran, E. C. 2002, ApJ, 565, 108

Freeman, P. E., Kashyap, V., Rosner, R., & Lamb, D. Q. 2002, ApJS, 138, 185

Gehrels, N. 1986, ApJ, 303, 336

Jansen, F., et al. 2001, A&A, 365, L1

Kilgard, R. E., Kaaret, P., Krauss, M. I., Prestwich, A. H., Raley, M. T., & Zezas, A. 2002, ApJ, 573, 138

Kubota, A., Done, C., & Makishima, K. 2002, MNRAS, 337, L11, (K01)

Kubota, A., Mizuno, T., Makishima, K., Fukazawa, Y., Kotoku, J., Ohnishi, T., & Tashiro, M. 2001, ApJ, 547, L119, (K01)

Lyons, L. 1991, Data Analysis for Physical Sciences (Cambridge, Cambridge University Press)

Maccacaro, T., Gioia, I. M., Wolter, A., Zamorani, G., & Stocke, J. T. 1988, ApJ, 326, 680

Mewe, R., Gronenschild, E. H. B. M., & van den Oord, G. H. J. 1985, A&AS, 62, 197

Mitsuda, K., et al. 1984, PASJ, 36, 741

Monet, D. G., et al. 2003, AJ, 125, 984

Okada, K., Dotani, T., Makishima, K., Mitsuda, K., & Mihara, T. 1998, PASJ, 50, 25, (O98)

Read, A. M., Ponman, T. J., & Strickland, D. K. 1997, MNRAS, 286, 626

Roberts, T. P., Goad, M. R., Ward, M. J., & Warwick, R. S. 2003, MNRAS, 342, 709

Saha, A., Claver, J., & Hoessel, J. G. 2002, AJ, 124, 839

Schinnerer, E., Böker, T., & Meier, D. S. 2003, ApJ, 591, L115

Shapley, A., Fabbiano, G., & Eskridge, P. B. 2001, ApJS, 137, 139

Stark, A. A., Gammie, C. F., Wilson, R. W., Bally, J., Linke, R. A., Heiles, C., & Hurwitz, M. 1992, ApJS, 79, 77

Strüder, L., et al. 2001, A&A, 365, L18

Sugiho, M., Kotoku, J., Makishima, K., Kubota, A., Mizuno, T., Fukazawa, Y., & Tashiro, M. 2001, ApJ, 561, L73

Tully, R. B. & Fisher, J. R. 1988, Catalog of Nearby Galaxies (Cambridge University Press, 1988)

Turner, M. J. L., et al. 2001, A&A, 365, L27

Vila-Costas, M. B. & Edmunds, M. G. 1992, MNRAS, 259, 121